BBA - Bioenergetics 1860 (2019) 78–88

Contents lists available at ScienceDirect

BBA - Bioenergetics

journal homepage: www.elsevier.com/locate/bbabio

Spectral microscopic imaging of heterocysts and vegetative cells in two filamentous cyanobacteria based on spontaneous Raman scattering and photoluminescence by 976 nm excitation

Kouto Tamamizu, Shigeichi Kumazaki*

Department of Chemistry, Graduate School of Science, Kyoto University, Kyoto 606-8502, Japan

ARTICLE INFO

Keywords:
Heterocystous cyanobacteria
Raman scattering microscopy
Anabaena variabilis
Rivularia
Photosystems
Thylakoid membranes

ABSTRACT

Photosynthetic pigment-protein complexes are highly concentrated in thylakoid membranes of chloroplasts and cyanobacteria that emit strong autofluorescence (mainly 600–800 nm). In Raman scattering microscopy that enables imaging of pigment concentrations of thylakoid membranes, near infrared laser excitation at 1064 nm or visible laser excitation at 488–532 nm has been often employed in order to avoid the autofluorescence. Here we explored a new approach to Raman imaging of thylakoid membranes by using excitation wavelength of 976 nm. Two types of differentiated cells, heterocysts and vegetative cells, in two diazotrophic filamentous cyanobacteria, *Anabaena variabilis*, and *Rivularia* M-261, were characterized. Relative Raman scattering intensities of phycobilisomes of the heterocyst in comparison with the nearest vegetative cells of *Rivularia* remained at a significantly higher level than those of *A. variabilis*. It was also found that the 976 nm excitation induces photoluminescence around 1017–1175 nm from the two cyanobacteria, green alga (*Parachlorella kessleri*) and plant (*Arabidopsis thaliana*). We propose that this photoluminescence can be used as an index of concentration of chlorophyll *a* that has relatively small Raman scattering cross-sections. The *Rivularia* heterocysts that we analyzed were clearly classified into at least two subgroups based on the Chl*a*-associated photoluminescence and carotenoid Raman bands, indicating two physiologically distinct states in the development or aging of the terminal heterocyst.

1. Introduction

The thylakoid membranes (TM) in chloroplasts of plants and algae or in cyanobacterial cells are highly enriched in the pigment-protein complexes containing photosynthetic pigments, majority of which are working for absorbing light and transferring electronic excitation energy to the reaction centers that drives the primary charge separations for the oxygenic photosynthesis [1,2]. Although the conversions from the fluorescent electronic excited states to the stable charge separated states are highly efficient (> 80%), the high concentration of the pigments enables one to study the photochemical events in the TM in live cells by observing autofluorescence from the photosynthetic pigments, especially chlorophyll *a* (Chl*a*) by various fluorescence microscopic techniques [3–7].

In fluorescence microscopy, the signal at a spatial point is generally given by the product of molecular concentration and fluorescence quantum yield. With an image of fluorescence intensity alone, the two quantities are inseparable. Fluorescence lifetime imaging microscopy (FLIM) can in principle indicate the two quantities separately as images of amplitude and (average) decay time constant of time-dependent fluorescence [3,8–11], but the former is still often distorted by position-dependence and wavelength dependence of reabsorption/scattering/reflection between the focus point of interest and microscope objective. The reabsorption effects are particularly serious for Chl*a* fluorescence because of its small Stokes shift [12,13]. On the other hand, spontaneous Raman scattering signal is proportional to the concentration of molecules [14]. It also suffers from reabsorption effects, but the Raman scattering signal can be tuned to wavelength regions with a high transmission like near infrared region by changing the excitation wavelength. One significant merit of Raman scattering for the imaging of TM is that non- or weakly fluorescent carotenoids are very sensitively detected and differentiated with highly characteristic fingerprints of molecular vibrational spectra [15–21]. Carotenoid molecules in TM play important roles in both light-harvesting and protective energy dissipation under strong light conditions [22–24].

Avoidance of autofluorescence around 600–800 nm region from

* Corresponding author.
E-mail address: kumazaki@kuchem.kyoto-u.ac.jp (S. Kumazaki).

https://doi.org/10.1016/j.bbabio.2018.11.012
Received 4 June 2018; Received in revised form 30 October 2018; Accepted 7 November 2018
Available online 08 November 2018

TMs can be commonly achieved by shorter or longer excitation wavelengths. The relatively short wavelength excitation should be favorable for resonance enhancements of the Raman scattering and resultant selectivities of target molecules [14,17]. One drawback of the resonance effects is excessive excitation that may result in disturbance of visible-light-induced physiological phenomena and/or damages in viability of cells [25,26]. Optical absorption of Chl*a*-based TM, especially by the absorption of photosystem I (PSI), seem to be extended up to at least 740 nm [27]. Recent studies have shown that excitations of PSI and photosystem II (PSII), both of which are the most essential Chl*a*-containing pigment-protein complexes in TM for the oxygenic photosynthesis, seem to be possible at least up to 840 and 820 nm, respectively [28–32]. Some previous works using spontaneous Raman scattering microscopy have reported bleaching effects of chloroplasts and cyanobacteria by 785 nm laser [33,34]. Plants, algae and cyanobacteria or their symbiotic forms in lichens have been, thus, often studied by 1064 nm laser excitation, by which autofluorescence is minimized [33,35–37]. Relatively high transmission and low scattering of the near infrared light through plant tissues full of photosynthetic pigments should be advantageous for imaging of deep tissues [38].

In this study, we have aimed at extending the range of possible excitation wavelengths for Raman (micro)spectroscopy by choosing a near-infrared (NIR) excitation at 976 nm. Excitation at 976 nm has several advantages over the one at 1064 nm. First, non-resonant Raman scattering cross-sections with excitation wavelength at 976 nm is about 40–50% greater than those at 1064 nm by the high frequency effects for the Stokes Raman scattering between 1000 and 2000 cm^{-1} [39]. Second, typical array detector or camera for the wavelength range of 0.9–1.6 μm is InGaAs sensors [40], with which Raman bands of higher vibrational frequencies can be obtained by 976 nm than by 1064 nm, especially when the quantum yield of the detector at the long-wavelength edge drops by cooling of the detector. One possible drawback of the 976 nm excitation is relatively high absorption by water in comparison with 1064 nm [41]. However, use of 976 nm beam certainly provides an additional degree of freedom in the design of microscope optics. For example, two beams of 976 and 1064 nm may be simultaneously used for different purposes like optical trapping of cells [42], inducing genes in cells by local heating [43], as well as Raman scatterings.

When some filamentous cyanobacteria sense a shortage of fixed nitrogen, approximately 1 in 10 to 20 vegetative cells differentiates into a heterocyst, in which oxygenic photosynthesis is suppressed through (at least partial) degradation of oxygen-evolving PSII while nitrogenase, nitrogen-fixing enzyme sensitive to oxygen, becomes operative [44–47]. On the other hand, the other cells, vegetative cells, continue oxygenic photosynthesis. The TMs in vegetative cells thus contain both PSI and PSII, while those in heterocysts contain predominantly PSI. The PSI in the heterocysts produce ATP by cyclic electron transport, because nitrogen fixation demands a large amount of ATP [31,45]. These drastic differences between heterocysts and vegetative cells have been frequently studied by fluorescence microscopy [4,31,48–51]. To the best of our knowledge, however, investigations on heterocyst-forming cyanobacteria by Raman scattering spectral microscopy have been relatively limited [52,53]. Here, we have successfully estimated the differences in amounts and/or concentrations of photosynthetic pigments between heterocysts and nearest vegetative cells in two genetically and morphologically distinct cyanobacteria, *Anabaena variabilis* and *Rivularia* M-261 [54]. It was unexpectedly found that 976 nm laser light actually induces a significant luminescence attributable to Chl*a* not only from the cyanobacterial cells but also from chloroplasts in a green alga and plant. Correlations between the Chl*a*-associated photoluminescence and Raman bands of carotenoids or phycobilins helped us understand the differences in pigment compositions between the two cyanobacteria and multiple physiological phases of *Rivularia* heterocysts.

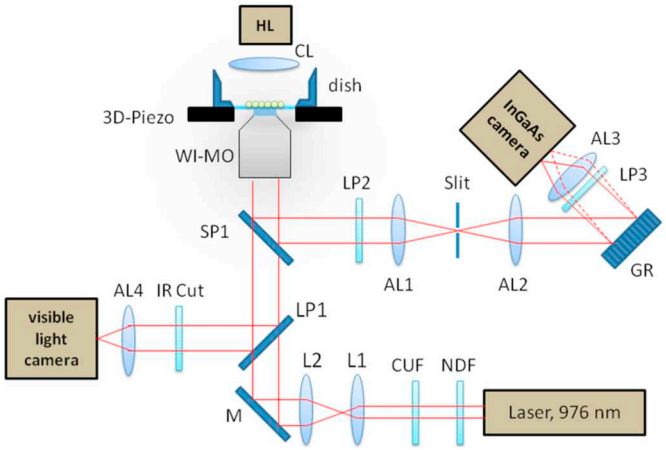

Fig. 1. Schematic diagram of the Raman microspectrometer. WI-MO: water-immersion microscope objective, AL1–AL3: achromatic lenses for the near infrared light, AL4: achromatic lens for the visible light, LP1: long-pass mirror with an edge wavelength of 900 nm, LP2 and LP3: long-pass filters with an edge wavelength at 980 nm, SP1: short-pass mirror with an edge wavelength of 1000 nm, M: mirror, GR: grating, CUF: narrow band transmission filter (laser clean up filter), NDF: neutral density filter, IR Cut: IR-absorbing filter, HL: halogen lamp, CL: condenser lens, L1 and L2: pair of lenses for a telescope, 3D-piezo: piezo actuator stage to move the sample positions, dish: glass-bottomed dish.

2. Experimental

2.1. Raman microspectroscopy based on 976 nm excitation

A schematic diagram of our deep NIR multichannel Raman microspectrometer is shown in Fig. 1. When samples were illuminated by a halogen lamp, the transmitted light through the short-pass dichroic mirror (SP1, edge wavelength (λ_{edge}) ≈ 1000 nm) was focused on a color CMOS camera (SILICON VIDEO 9M001, EPIX, Illinois, USA) after reflection by a long-pass dichroic mirror (LP1, λ_{edge} ≈ 900 nm) for a bright-field imaging in the visible region. A narrow-band diode laser (center wavelength of 976 nm, frequency band width < 1 MHz, I0976SA0200B-THTK, Innovative photonics solutions) was used as the excitation source for the Raman scattering. The 976 nm laser beam, after transmission through a spectral clean-up (CUF) and neutral density filters (NDF), was first magnified by a telescope and focused onto a sample with a water-immersion microscope objective lens with a magnification of ×60 and numerical aperture of 1.27 (Nikon, CFI PlanApo IR60XWI). Raman scattering signals were collected by the same objective lens. The short-pass mirror (SP1) reflected the signals toward a home-made achromatic-lens-based imaging polychromator with a focal length of 250 mm and 1:1 magnification. The entrance slit of the polychromator was set to be 0.12 mm width. The blaze wavelength of the grading was 1000 nm or 1200 nm and the number of grooves was 300/mm (Thorlabs GR50-0310 or Photon Design, Tokyo, Japan). An electrically cooled InGaAs camera (−80 °C, 640 × 512 pixels, pixel size = 20 × 20 μm, DMDIR-640, Photon Design, Tokyo) was fixed at the exit port of the polychromator. Residual laser light was rejected by two long-pass filters (LP2 and LP3, λ_{edge} ≈ 980 nm) that were located outside and inside the polychromator. The laser power at the sample position was most typically 10–14 mW unless otherwise specified. In the imaging measurement, the sample was horizontally and/or vertically translated by a piezoelectric stage (PK3L150-100UA, Nanocontrol, Tokyo) with a typical step of 0.4 μm and 1.0 μm, respectively. At each spatial point, one Raman scattering spectrum was obtained with an exposure time of 2.0 s.

2.2. Cyanobacterial cells, unicellular green alga and plant leaf

A filamentous cyanobacterium, *Anabaena variabilis* (*A. variabilis* strain NIES-2095), was purchased from the microbial culture collection at the National Institute of Environmental Studies in Tsukuba, Japan. The filamentous cells were grown photoautotrophically under fixed-nitrogen-deprived conditions in a nitrogen-free BG-11 liquid medium [55] for 5 to 76 days at 29 °C with a 15-h-light/9-h-dark photoperiod. The medium was prepared by removing $NaNO_3$ and replacing ferric ammonium citrate with ferric citrate in the BG-11 formulation. The flux density of photosynthetic photon at the sample position in the incubator was about 20 μmol photons $m^{-2} s^{-1}$.

Rivularia sp. IAM M-261 was obtained from the culture collection of Institute of Molecular and Cellular Biosciences, the University of Tokyo (IAM Collection), which has been transferred to Microbial Culture Collection at the National Institute for Environmental Studies (NIES Collection Tsukuba, Ibaraki, Japan). *Rivularia* filaments were grown on agar media based on the nitrogen-free BG-11 at about 20 μmol photons $m^{-2} s^{-1}$ without any dark period for 9 to 23 days. Both *A. variabilis* and *Rivularia* cells were precultured in the fixed-nitrogen-free BG11 media for longer than 14 days and inoculated to fixed-nitrogen-free BG11 media that were maintained for the above-mentioned durations until the microscopic observations.

Unicellular green alga, *Parachlorella kessleri* (*P. kessleri*), was purchased from the IAM culture collection as IAM C-531 (now maintained as NIES-2160). The cells were grown photoautotrophically in 40 cm^3 of BG-11 liquid medium (including fixed nitrogen) in the same incubator as *A. variabilis*. The preparation for the microscopic observation was also the same as used for *A. variabilis* cells. *Arabidopsis thaliana* plants were grown in soil in chambers at 21–23 °C under a 12-h-light/12-h-dark photoperiod using fluorescent lamps (about 100 μmol $m^{-2} s^{-1}$).

For the Raman microscopic imaging of *A. variabilis* and chloroplasts of green alga (*P. kessleri*), the cell suspensions were transferred to glass-bottomed dishes (Matsunami, D111505). The upper surface of the glass was coated with poly-L-Lysine to immobilize the cells before addition of the cell suspensions. About 10 min after the cell suspension was added, a block of solidified growth-medium-based agarose was put on the adsorbed cells to fix the cells better. In the case of *Rivularia*, a piece of agar block was transferred from the agar plates to the cover-glass-bottomed dishes for observing cells on the agar surface.

For microscopic imaging of *A. thaliana* chloroplasts, one green leaf was sandwiched by a cover glass (No.1, Matsunami) and optical window with a thickness of 1.0 mm. A home-made aluminum sample holder was used to fix the leaf and two glass plates with a help of Teflon spacers. The internal space of the sample holder was filled with tap water. Microscopic observations of chloroplasts in mesophyll cells of *A. thaliana* leaf were conducted from the adaxial surface.

2.3. Reference pigments and pigment-protein complex

Raman scattering spectra of representative photosynthetic pigments and pigment-protein complexes were obtained by using powders of β-carotene (Nacalai tesque, 07312-81), C-phycocyanin (from *Spirulina*, Sigma-Aldrich, P2172), and Chl*a* (Wako Pure Chemical Industries, 034-21361). These were used as received by placing them between cover and slide glass plates, in the same sample holder as used for the *A. thaliana* leaf.

3. Results

3.1. Raman scattering spectral imaging of Anabaena variabilis cells

The bright field image of some filaments of *A. variabilis* grown in the fixed-nitrogen-depleted medium typically showed a terminal heterocyst that was located at the end of the filament (designated as het in Fig. 2A or S1B). The heterocyst was connected to vegetative cells (in the order of het, veg1, veg2, veg3, as in Fig. 2A). The heterocyst was characterized by a higher optical transmission than the vegetative cells, because of a decrease in the amount of photosynthetic pigments, especially phycobilisome [31,49,54,56]. The total intensity of the Raman scatterings and/or photoluminescence signals integrated over all detected wavelength range (1017–1175 nm) was calculated in each pixel and shown as a monochromatic image (Fig. 2B). It should be noted that the heterocyst and vegetative cells were comparable in the brightness of the total Raman scattering and photoluminescence signals. This is in contrast to conventional fluorescence images of heterocysts and neighboring vegetative cells of filamentous cyanobacteria (including *A. variabilis*), in which fluorescence of heterocyst is far weaker than that of vegetative cells [10,31,49,54].

Raman scattering signals of individual single cells were extracted semiautomatically in an analogous way that was previously described for fluorescence spectral microscopy (Fig. 2C) [54]. The average Raman spectra of heterocysts and vegetative cells that were obtained from 31 *A. variabilis* filaments, each containing one heterocyst (only one filament contained intercalary heterocyst, see Fig. S1), are shown in Fig. 3. The Raman band assignments were mainly based on the Raman spectra of the powders of β-carotene, C-phycocyanin (phycobilin-protein complex) and Chl*a* (Fig. 4A–D) obtained with the same setup, which seemed to be consistent with several references (Table S1) [33,57–59]. The phycobilin bands that were clearly visible in vegetative cells were almost totally absent in the heterocysts (Figs. 2F and 3). The carotenoid bands were slightly decreased in the heterocysts in comparison with the vegetative cells (Figs. 2E and 3). The Raman scattering spectra of both the heterocysts and vegetative cells were superimposed on a broad photoluminescence spectrum (Fig. 3). The spectral features of het, veg1 and veg2 were thus consistent with the selective images of individual Raman bands and photoluminescence (Fig. 2D–F). Although at least three Raman bands were ascribed to Chl*a* in the average spectra of the 31 cells (Fig. 3), the signal-to-noise ratios of the single Raman bands were insufficient to produce Chl*a* selective image with a reasonable contrast.

3.2. Raman scattering spectral imaging of Rivularia cells

Analogous analysis was also performed on Raman/photoluminescence spectra of 34 *Rivularia* filaments. Only major differences between *A. variabilis* and *Rivularia* are described here. In terms of relative signals of the heterocysts in comparison with the nearby vegetative cells, photoluminescence signals in *Rivularia* heterocysts were on average weaker than those of *A. variabilis* (Tables 1, 2, Figs. 2D, J, 3, S2). Phycobilin Raman signals in *Rivularia* heterocysts were stronger than those of *A. variabilis* (Tables 1, 2, Figs. 2F, L, 3, S2). The latter feature is consistent with our previous study with microscopic absorption spectroscopy showing that there remains a substantial amount of phycocyanin in the *Rivularia* heterocysts, while mature heterocysts of *A. variabilis* are virtually free from phycobilisomes [54].

3.3. Photoluminescence of the cyanobacterial cells excited by 976 nm is attributable to chlorophyll a

The Raman spectrum of β-carotene was virtually free from any broad luminescence component (Fig. 4A). C-phycocyanin is a subunit of phycobilisome that works as extra light-harvesting antenna mainly for PSII but also for PSI [60,61]. Although C-phycocyanin containing phycobilins as light-harvesting chromophores showed some broad photoluminescence superimposed on the narrow banded Raman signals, the intensity ratio of luminescence to Raman of C-phycocyanin seemed to be far lower than that of Chl*a* (Fig. 4B, C). Moreover, phycobilin contribution to the photoluminescence of the *A. variabilis* cell can be estimated as follows. After magnification of the heterocyst spectrum by 1.59 in Fig. 3, the normalized spectrum becomes very similar to that of veg1, except in the wavelength regions in which

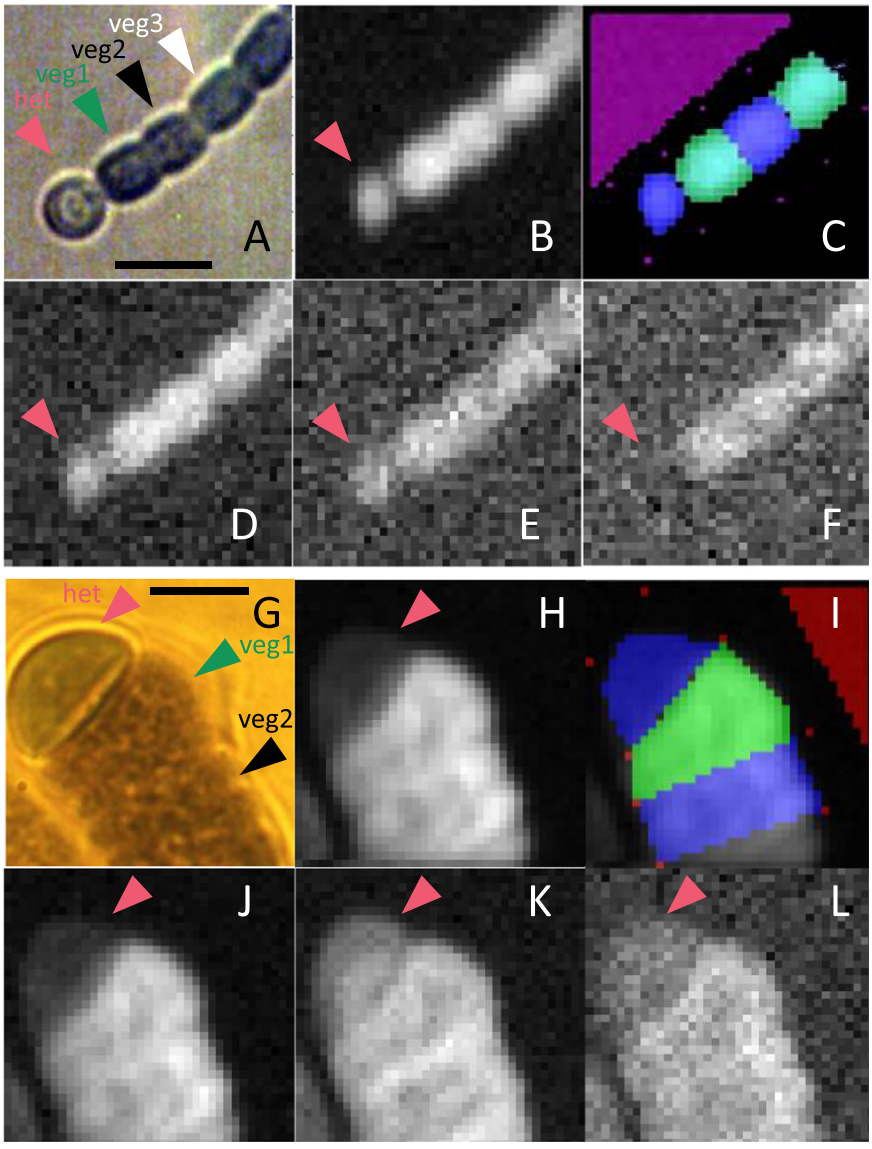

Fig. 2. Typical microscopic images of a filament of *A. variabilis* (A–F) and *Rivularia* cells (G–L). (A, G) Bright field image of a filament with a heterocyst at the terminus. The colors of these images are artificial due to applications of auto-contrast and auto-level functions of a software (XnView) and yellowish illumination of the halogen lamp, while the darkness of the pixels reflects absorption, reflection, and scattering at some visible wavelengths of the cells. The magenta arrow head indicates a heterocyst, and the vegetative cells marked by the three arrow heads of green, black and white are designated veg1, veg2 and veg3, respectively. Scale bar = 5 μm in both (A) and (G), which is also applicable to the other panels. (B, H) Image of the total intensity of Raman scattering and photoluminescence signals integrated over all the detected wavelength range. (C, I) Map of selected areas of individual cells for spectral analysis. Blue and green regions alternately show selected regions of individual cells. The triangular area in purple (in C) or red (in I) shows a cell-free background region. Four magenta points surrounding individual cells were given by visual inspections, and they worked as reference points to locate cell junctions. (D, J) Image of the photoluminescence detected in the Raman shift range between 1707 and 1736 cm^{-1} (between 1171 and 1175 nm in wavelength). (E, K) Image of a carotenoid Raman band between 1513 and 1528 cm^{-1}. (F, L) Image of a phycobilin Raman band between 1618 and 1633 cm^{-1}. For both (E, F) and (K, L), photoluminescence signals were subtracted (see Fig. S3).

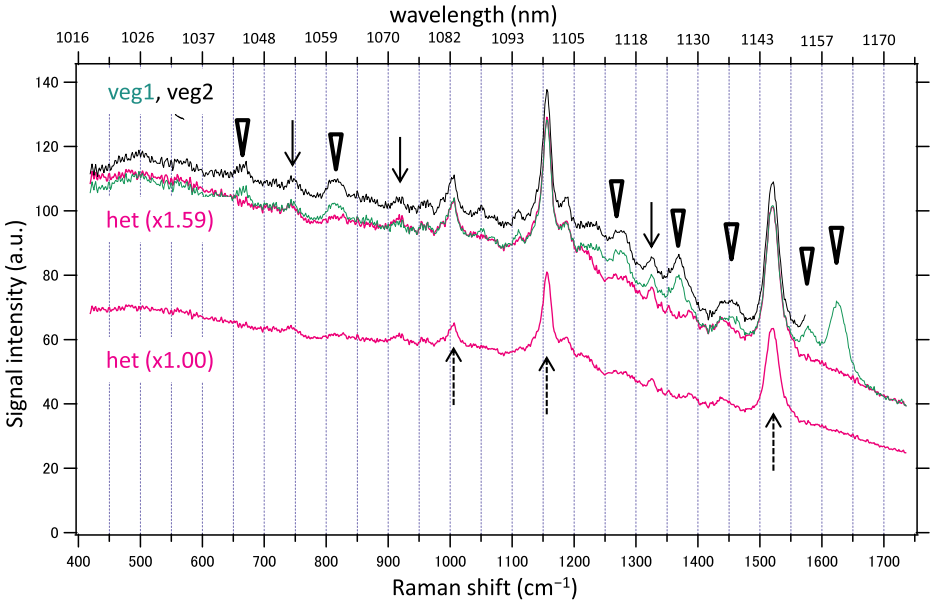

Fig. 3. Cell-type specific average single-cell spectra of *A. variabilis* cells in which Raman scattering and photoluminescence signals are present. The intensities of the spectra are based on the "whole-cell-integrated intensities" in the Tables 1 and S2, which are functions of cell sizes. The two plots in magenta represent average spectra of heterocysts, among which one spectrum (het (×1.59)) is magnified by 1.59 times from the other spectrum (het (×1.00)) preserving the original intensities. The plot in green (veg1) represents the vegetative cell that is directly adjacent to the heterocysts. The plot in black (veg2) indicates the vegetative cell that is directly adjacent to veg1 but not to heterocyst (see Fig. 2A). Upward arrows with broken lines, downward arrows with solid lines and downward triangular arrow heads indicate Raman bands attributable to carotenoids, Chl*a* and phycobilin molecules, respectively. See Table 1 for cell-by-cell variations of signal intensities.

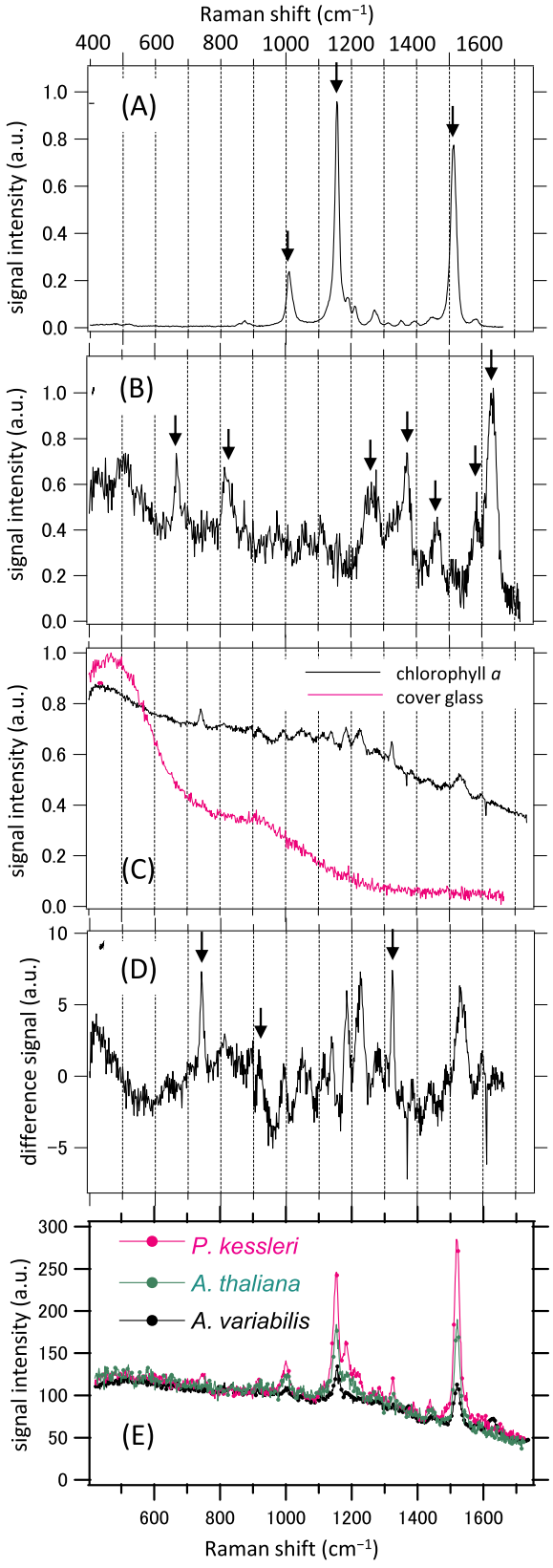

Fig. 4. Raman scattering and photoluminescence spectra of powders of photosynthetic pigments, cover glass, cyanobacterial cells and chloroplasts of green alga and plant that were obtained with excitation at 976 nm. (A) β-Carotene, (B) C-phycocyanin, (C) Chl*a* and cover glass. In (D), the same spectrum of Chl*a* in (C) is shown after a broad photoluminescence spectrum was subtracted. The luminescence spectrum contained in the Chl*a* spectrum was approximated by a seventh-degree univariate polynomial fitted to the whole Chl*a* spectrum in (C). The Raman bands marked by arrows in (A), (B) and (D) indicate those that are marked by the arrows or arrow heads in the cell-type specific spectra in Fig. 3. (E) Comparison of the average Raman and photoluminescence spectra of *Parachlorella kessleri* cells (two cells) in magenta, two chloroplasts inside a mesophyll cell in a leaf of *Arabidopsis thaliana* in green and vegetative cells in five filaments of *A. variabilis* in black. The three spectra were arbitrarily magnified so that the broad photoluminescence components overlap with each other.

C-phycocyanin Raman bands are prominent (cf. Fig. 4B). Given the nearly total disappearance of phycobilins Raman bands in the transition from the vegetative cells to the heterocysts, this situation indicates that photoluminescence of phycobilisome does not contribute to the observed broad photoluminescence of the *A. variabilis* cells. Overall, the whole situation is best represented by the idea that photoluminescence in both the vegetative cells and heterocysts of *A. variabilis* is exclusively attributable to Chl*a*.

It should be here noted that some photoluminescence was also observed when the 976 nm laser focus was near the cover glass (plot in magenta, Fig. 4C) [62,63], which probably indicates impurities, defects, and/or doped elements in the glass [64]. The spectral shape of the cover glass luminescence was clearly different from those of Chl*a* and cyanobacterial cells (Figs. 3, 4C). Its contribution to the Raman scattering/photoluminescence spectra of the reference chemicals and cells was always subtracted before analysis (see caption of Fig. S3).

3.4. Single cell amount and average intracellular concentration of photosynthetic pigments in the neighboring cells

The intensities of the Raman bands of β-carotene and phycobilins as well as the photoluminescence attributable to Chl*a* were estimated from the Raman spectra of single cells or single pixels in the way described in the caption of Fig. S3. The axial spatial resolution of our Raman microscopy setup was well approximated by a Gaussian function with a full width at half maximum of 3.7 μm (Fig. S4), which was comparable to the thickness of the *A. variabilis* cells (≈2–4 μm, Figs. 2A–F and S1). It is thus concluded that the Raman signal intensity of an *A. variabilis* image per single pixel (corresponding to I_{sig} in Table 1) is largely proportional to the integrated amount of pigments along the depth axis (z axis, which is perpendicular to the plane of the images in Fig. 2A–F). The integration of the signals in the whole two-dimensional area (S_{cell}) of an *A. variabilis* cell (as in the case of the spectra in Fig. 3 and corresponding to $I_{sig} \times S_{cell}$ in Table 1), thus, reflects the whole single-cell amount of the pigments. Average concentration of a pigment inside the *A. variabilis* cell is approximately proportional to the average signal intensity per single pixel divided by the thickness of the cell (corresponding to $I_{sig} \times (S_{cell})^{-1/2}$ in Table 1), as far as we neglect the heterogeneous distribution of TM in the *A. variabilis* cell. The above-mentioned three quantities reflecting integrated amounts or concentrations of photosynthetic pigments in the specified cell types (heterocyst and veg1, see Fig. 2A) are summarized in Table 1, after they were normalized by the corresponding quantities in veg2 (see Fig. 2A and Table S2 for veg3).

Among the three connected cells designated as het, veg1, veg2, and veg3 (Fig. 2A), the *A. variabilis* heterocyst showed the least amount of photosynthetic pigments (Tables 1 and S2). Relative amount of phycobilins in heterocyst on average was only 6% of veg2 cell. Because of the signal-to-noise ratio and unavoidable arbitrariness in the subtraction of photoluminescence background, we regard this 6% as an upper limit of the phycobilin amount on average (Fig. S3). The nearly complete disappearance of phycobilin was in good agreement with our own previous study on *A. variabilis*, in which heterocysts and its neighboring vegetative cells were analyzed by microscopic absorption spectroscopy

Table 1
Ratio of Raman band and luminescence intensities of specified cell types to the corresponding values of veg2 (vegetative cell) in the same *A. variabilis* filament, for which at least three consecutive cells, one heterocyst and two vegetative cells (het, veg1, and veg2) were imaged by our spectro-microscope (e.g., Fig. 2A). Number of analyzed filaments was 31 including the 21 filaments analyzed in the Supplemental Table S2. See the captions of Figs. 2 and S3 for the selected Raman shift or wavelength regions. According to paired *t*-tests with the corresponding values of the veg2 cell in the same filament, statistical significance is indicated by the following symbols. *: $p < 0.05$, **: $p < 0.01$, ***: $p < 0.005$, ****: $p < 0.001$, #: $p < 0.0005$, ##: $p < 0.0001$. Even smaller p values are not distinguished.

Component	Cell type	Whole-cell integrated intensity (± s.e.), $I_{sig} \times S_{cell}$	Average intensity per single pixel in the region occupied by TM (± s.e.) I_{sig}	Average intensity per unit volume occupied by TM (± s.e.) $I_{sig} \times (S_{cell})^{-1/2}$	Average cross-section of TM-occupied region in the image (± s.e.) S_{cell}
Luminescence	het	0.584## (± 0.066)	0.733## (± 0.046)	0.878* (± 0.045)	0.733# (± 0.058)
	veg1	0.936 (± 0.054)	0.940* (± 0.023)	0.964 (± 0.023)	0.984 (± 0.046)
Carotenoid	het	0.599## (± 0.051)	0.826## (± 0.026)	1.073 (± 0.081)	
	veg1	0.915 (± 0.052)	0.922*** (± 0.022)	0.950 (± 0.026)	
Phycobilin	het	0.063## (± 0.009)	0.090## (± 0.013)	0.095## (± 0.014)	
	veg1	0.896* (± 0.049)	0.903## (± 0.016)	0.929*** (± 0.021)	

[54]. Although a small portion of PSII may remain in the heterocysts [4,10,31,47], degradation of PSII during the heterocyst differentiation of *A. variabilis* seems to be accompanied by nearly complete degradation of its light-harvesting phycobilisomes containing phycobilins. Statistically significant differences were found between veg1 and veg2 (Tables 1 and S2) of *A. variabilis*. The differences between veg2 and veg3 were less significant than those between veg1 and veg2. To the best of our knowledge, such gradients in the properties of TM of vegetative cells near heterocysts have not been reported previously for *Anabaena* and genetically similar *Nostoc* [65].

In the case of *Rivularia* cells, the thickness (dimension perpendicular to filament axis) near the heterocyst terminal was typically 7–10 μm (Figs. 2G, S1), which was longer than the above-mentioned full width at half maximum of the axial point-spread function (3.7 μm). Given the imaging at only a single depth under these conditions, only "whole-TM-cross-section-integrated intensity" and "average intensity per single pixel in the region occupied by TM" were given as in Table 2.

3.5. Correlations among pigments in the same cell

Correlation among intracellular pigment concentrations were analyzed on the basis of average intensities per single pixel in the TM-occupied regions of single cells (Fig. 5, c.f. Fig. S5). In the case of the vegetative cells of both *A. variabilis* and *Rivularia*, moderate to high correlations ($r \approx 0.4$–0.8) were found in all three combinations. This must reflect a certain level of stability in ratios among PSI, PSII and phycobilisome in the vegetative cells under our growth conditions as well as those of photosynthetic pigments in the individual pigment-protein complexes of PSI, PSII (see also Tables S3, S4).

In the heterocysts of *A. variabilis*, low or almost no correlation was found among all three combinations ($-0.22 < r < 0.11$ in Fig. 5A–C). The low correlations associated with phycobilins are understandable, because most phycobilisomes are degraded in matured *A. variabilis* heterocyst [54]. Remaining phycobilisomes in the heterocysts of *A. variabilis*, if any, are probably not forming stable complex with PSI. On the other hand, the low correlation between Chl*a*-associated photoluminescence and carotenoid in the *A. variabilis* heterocyst ($r = -0.003$) cannot be explained by only the changes in the stoichiometry of PSII and PSI between vegetative cells and heterocysts (Tables S3, S4). It is noteworthy that a high correlation coefficient was found if these signals were plotted on the basis of whole-cell integrated intensities (Fig. S5A). The correlation plots in Fig. 5 are thus substantially free from effects coming from cell sizes.

Compared to *A. variabilis* heterocyst, substantially higher correlations in all three combinations were found in the case of *Rivularia* heterocyst ($0.470 \le r \le 0.793$ in Fig. 5D–F). These are at least in part explained by the PSI-phycocyanin complex previously found in the *Rivularia* heterocysts [54,61]. It is to be noted that there seem to be at least two distinct subgroups of *Rivularia* heterocysts in terms of the ratio of the photoluminescence to carotenoid signals (Fig. 5D). One subgroup of heterocysts was aligned near the line in which Chl*a*/carotenoid ratio in the vegetative cells are conserved (the diagonal line, y = x in the Fig. 5D), while the other was aligned near the line in which luminescence/carotenoid ratio is about 0.35 (magenta line with a relatively low

Table 2
Ratio of Raman band and luminescence intensities of specified cell types to the corresponding values of veg2 (vegetative cell) in the same *Rivularia* filament. The definitions of signals and symbols are the same as in Table 1, unless otherwise mentioned. Total number of analyzed filaments was 34, and they were classified into two subgroups of A ($N = 16$) and B ($N = 18$) according to photoluminescence/carotenoid Raman intensity ratio (see Figs. 5D, S2, S7). See Fig. 2G in the main text for the notations of het, veg1, and veg2.

Component	Cell type	Subgroup	Whole-TM-cross-section-integrated intensity ($I_{sig} \times S_{cell}$)	Average intensity per single pixel in the region occupied by TM (I_{sig})	Average cross-section of TM-occupied region in the image (S_{cell})
Luminescence	het	all(1)	0.277 (± 0.034)##	0.452 (± 0.044)##[##(3)]	0.609 (± 0.050)##
		A(2)	0.408 (± 0.048)##(2)	0.665 (± 0.052)## (2)	0.653 (± 0.077)
		B(2)	0.161 (± 0.029)##(2)	0.262 (± 0.019)## (2)	0.569 (± 0.061)
	veg1	all(1)	1.05 (± 0.090)	0.923 (± 0.018)#	1.12 (± 0.082)
Carotenoid	het	all(1)	0.440 (± 0.041)##	0.731 (± 0.032)##[*(3)]	
		A(2)	0.448 (± 0.051)	0.728 (± 0.048)	
		B(2)	0.433 (± 0.064)	0.732 (± 0.044)	
	veg1	all(1)	1.06 (± 0.086)	0.946 (± 0.015)***	
Phycobilin	het	all(1)	0.311 (± 0.034)##	0.528 (± 0.041)##[##(3)]	
		A(2)	0.358 (± 0.053)	0.622 (± 0.077)*(2)	
		B(2)	0.270 (± 0.044)	0.446 (± 0.027)*(2)	
	veg1	all(1)	1.05 (± 0.082)	0.938 (± 0.018)*	

Notes: (1) When all *Rivularia* filaments are concerned, statistically significant differences between het and veg2, or between veg1 and veg2, are shown in the same way as in the case of *A. variabilis* (Tables 1 and S2).
(2) The statistical significance associated with the subgroups A or B were given by t-tests between the heterocysts of the subgroups A and B.
(3) The symbols in the bracket, like [##], indicate statistically significant differences in the heterocyst between Rivularia and *A. variabilis*.

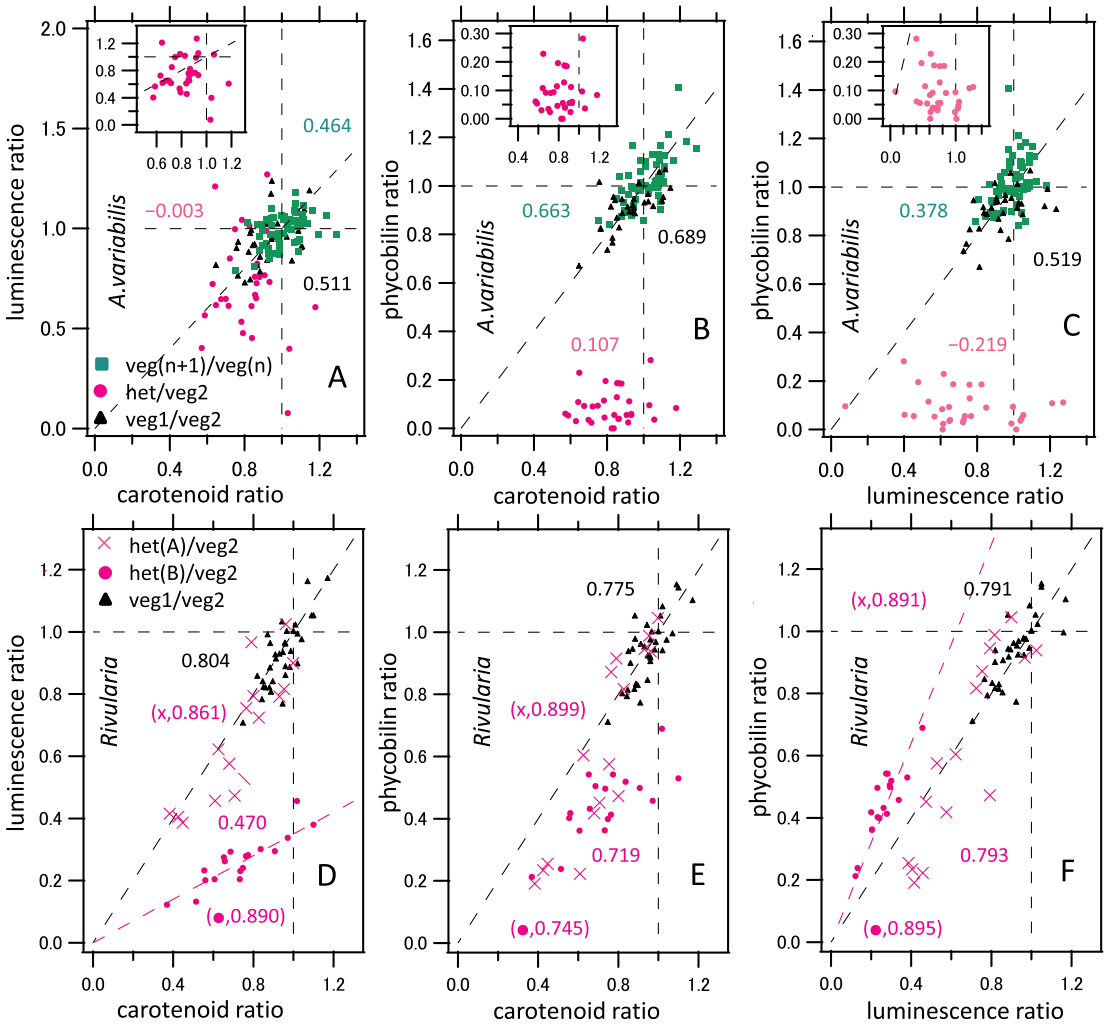

Fig. 5. Correlation plots between pigments in the same cell of *A. variabilis* (A–C) and *Rivularia* (D–F). All plotted relative intensities are based on the "average intensities per pixel (in the region occupied by TM)" as shown in Tables 1 and 2. See the captions of Fig. 2 or S3 for the selected Raman shift or wavelength regions. The quantities of the heterocysts and veg1 cells are normalized by those in veg2 in the same filament. Only in the case of *A. variabilis*, pairs of neighboring vegetative cells designated as veg(n + 1) and veg(n) were analyzed, in which the two cells were far from heterocysts in relatively long filaments grown under the fixed-nitrogen-deprived conditions. The inserted graph in (A–C) shows the plot for het/veg2 in an approximately square frame. In (D–F), *Rivularia* heterocysts were classified into two subgroups A and B (het(A)/veg2 and het(B)/veg2), according to the ratio of Chl*a*-associated photoluminescence and carotenoid Raman intensity (see Section 3.5 and Fig. S7). In all panels, numbers in the graphs are correlation coefficients. In (D–F), correlation coefficients for the subgroups A and B are shown separately by the numbers in brackets. Broken lines in black or magenta are reference lines indicating y = 1 (horizontal), x = 1 (vertical), y = x (approximately or rigorously diagonal), y = 0.35x (magenta, in D) and y = 1.6x (magenta in F).

gradient, y = 0.35x in the Fig. 5D). Based on the luminescence/carotenoid signal ratio, *Rivularia* heterocysts were classified into two subgroups A and B, in which heterocysts of the subgroup A were located above y = 0.6x and those of the subgroup B were located below y = 0.5x in the Fig. 5D (see also Fig. S7). The two subgroups of heterocysts are also well separated in the phycobilin Raman/Chl*a*-associated photoluminescence correlation plot (Fig. 5F). Differences in the average values of the two subgroups are summarized in Table 2, and representative average single-cell spectra are shown in Fig. S2.

3.6. Laser power dependence of the photoluminescence

The excitation mechanism leading to the photoluminescence of the cyanobacterial cells was also investigated through laser power dependence of the signal amplitude in the case of *A. variabilis* (Table S6). Contribution ratios of apparently one-photon and two-photon excitations at 13.5 mW was estimated to be between 77:23 and 53:47 in five spectral regions that were relatively free from obvious Raman components. It is noteworthy that one-photon excitation at 976 nm is not negligible at all.

3.7. Photoluminescence of chloroplasts of plant and green alga induced by the 976 nm continuous wave excitation

The TMs in the chloroplasts of plants and eukaryotic green algae are also highly enriched in Chl*a* [12]. The generality of the broad photoluminescence attributed to Chl*a* in the above section was also tested by applying the same spectromicroscopic setup to the chloroplasts in unicellular green alga (*Parachlorella kessleri*) and in leaves of a model plant (*Arabidopsis thaliana*). The spectral shapes of the broad photoluminescence of the plant and green alga were very similar to that of cyanobacterium *A. variabilis* (Fig. 4E). In the cases of the plant and green alga, the ratios of the integrated intensities of the carotenoid Raman bands at around 1520 cm^{-1} to the photoluminescence background at the same wavelength region are estimated to be 2.6 and 4.2 times greater than that of cyanobacterial vegetative cell, respectively. See Text S1 for possible interpretations of this ratio.

4. Discussion

4.1. Comparison with previous absorption spectral microscopy

Microscopic absorption spectra of heterocysts and neighboring vegetative cells in the two cyanobacteria, *A. variabilis* and *Rivularia*, were previously analyzed [54]. The relative photoluminescence intensities of *A. variabilis* heterocyst in comparison with veg2 in this work are very similar to the corresponding values of the microscopic absorbance attributed to Chl*a* that were given by the spectral decomposition of single-cell absorption spectra in the previous work (Tables 1, S7). This leads us to propose that the intensity of the spectrally broad photoluminescence induced by the 976 nm continuous wave laser is fairly proportional to the concentration of Chl*a*.

It should be noted here that possible sensitization of the Chl*a* photoluminescence by phycobilins in the phycobilisome of vegetative cells in *A. variabilis* is excluded by the above-mentioned high correlation between the Chl*a* absorbance and the photoluminescence. Possible sensitization of the Chl*a* photoluminescence by Chl*b* and/or carotenoids in the cyanobacterium, green alga and plant is discussed in the Supplemental Text S1.

On the other hand, the average decrease of Chl*a* absorption from the veg2 to heterocyst in *Rivularia* filaments in the previous microscopic absorption microspectroscopy (≈28%) was comparable to that in the photoluminescence intensity of the heterocyst subgroup A in this work (≈34%), which is, however, far milder than that in the subgroup B (≈74%) (Tables 2, S8) [54]. Given the presence of at least two subgroups of *Rivularia* heterocysts with clearly different spectral characters (Figs. 5D, S7), it is possible that the samplings of heterocysts in the previous absorption microscopy and this work may have been somehow differently biased.

4.2. Mechanisms and implications of photoluminescence from chlorophyll a in the thylakoid membrane

Linear portion of the photoluminescence in terms of the laser power dependence (Table S6) is possibly attributable to spin-forbidden but actually very weakly allowed transitions between S_0 and T_1. Phosphorescence spectrum of Chl*a* in mature pea leaves at 77 K has been reported to have a main peak around 980–990 nm and a vibronic progression peaking around 1100 nm [66]. On the other hand, it is also possible that long-wavelength tail (vibronic progression) of the fluorescence bands ($S_1 \rightarrow S_0$, main bands are peaking around 670–730 nm depending on the spectral forms of Chl*a* in cyanobacteria) give substantial contributions to the detected photoluminescence (1017–1175 nm) in our study [63]. The nonlinear portion of the detected photoluminescence (Table S6) can be attributable to the fluorescence of Chl*a*, because the high intensity of the focused 976 nm laser may induce two-photon direct excitation of some photosynthetic pigments and/or multistep excitations consisting of heating effects by the laser (generation of vibrationally excited states in S_0 (hot S_0)) and single-photon excitation (hot $S_0 \rightarrow S_1$). The heating can be caused by absorption of the 976 nm photon at least in part by the water in the case of the cyanobacterial cells [41], but there is no water in the Chl*a* powder (Fig. 4C). In the case of the powder of Chl*a*, lattice vibrations of the powder as well as combinations and/or overtones of molecular vibrations of the individual Chl*a* may contribute to absorption of 976 nm and rise of the local (vibrational) temperature.

The clear photoluminescence from matured *A. variabilis* heterocysts (Table 1, Figs. 2D, 3, 5A) readily supports an idea that PSI is a strong emitter of this photoluminescence under our experimental conditions. Some discussion on relative contributions of PSI and PSII to the photoluminescence is given in the Supplemental Text S1.

4.3. Side effects of the 976 nm excitation

The photoluminescence of Chl*a* implies two possible disadvantages of using the 976 nm laser for imaging of TM, as discussed in Section 4.2. One is the possible production of harmful triplet excited states of Chl*a* leading to generation of singlet oxygen ($^1O_2$) [67]. The other is the heating of water molecules, which should be certainly more substantial than those at 1064 nm [41]. We may have to avoid using the 976 nm excitation laser for repetitive examinations of physiological phenomena of photosynthetic organisms, although long-term observations of organisms after the 976 nm excitation remains to be performed. When the laser power at the sample position was 20 mW or even higher, we sometimes found bleaching of photosynthetic pigments of *A. variabilis* cells and/or obvious changes of the cell shapes. On the other hand, pinpoint production of triplet states of pigments and/or singlet oxygen may be useful for analyzing possible roles of signaling by such molecular species as well as protection mechanisms of the photosynthetic systems against harmful chemicals [68].

4.4. Properties of the heterocysts of Rivularia and Anabaena variabilis

Rivularia filaments were subcultured from a densely populated agar medium to a freshly prepared one, which seemed to stimulate development of hormogonia (relatively short motile filaments for the dispersal and relocation of the microorganism) from parental filaments (Fig. S1) [69]. Even though the *Rivularia* filaments had been subcultured over several agar media that did not originally contain fixed nitrogen, hormogonia did not have obvious heterocysts. Hormogonia are generally thought to consist of undifferentiated cells [70]. It is thus possible that the terminal cells at the heterocyst position of *Rivularia* analyzed in this study were situated at various transition stages from a transient terminal vegetative cell to a matured heterocyst. Among the two subgroups of *Rivularia* heterocysts (Table 2, Figs. 5D–F, S7), the signal ratios of photoluminescence/carotenoid of the subgroup A are similar to those of nearby vegetative cells. It is thus likely that the heterocysts in the subgroup B are more matured ones and that those in the subgroup A are relatively young heterocysts. The signal ratios of phycobilins/photoluminescence of the subgroup B (postulated mature heterocysts) are higher than those of subgroup A (postulated young heterocysts). This trend is contrary to the one in *A. variabilis*, in which phycobilins/photoluminescence ratio is clearly lower in heterocysts than in vegetative cells (Fig. 5C). This situation probably reflects two factors: (i) a high portion of PSI in the *Rivularia* heterocysts is bound to phycocyanin [54], and (ii) Chl*a* contents in the heterocyst subgroup B (matured heterocyst) were on average lower than those in the subgroup A (young heterocyst) (Table 2, Fig. S3). Based on our proposal that Chl*a* concentration, as measured by microscopic absorbance per unit depth [54], is approximately proportional to the Chl*a*-associated photoluminescence (Table S6), differences between heterocysts and vegetative cells of the *Rivularia* leads to the idea that the heterocysts in the subgroup A observed here are similar to those analyzed in our previous study (Table S8) [54]. Although the heterocysts in the subgroup A seem to be relatively young in comparison with the subgroup B, their absorption and fluorescence features including PSII/PSI fluorescence intensity ratio may be sufficiently distinct from those of vegetative cells [54]. It is noteworthy that so many young heterocysts (16 among 34) were clearly separated from matured heterocysts by the spectroscopic indices, which suggests a relatively long lifetime of the young stage of the heterocysts and swift drastic change in the intracellular pigments at certain maturation/aging stages.

The low ratios of Chl*a*-associated photoluminescence to carotenoid in the subgroup B of *Rivularia* heterocyst (postulated matured heterocysts) in comparison with the vegetative cells (~0.35:1, Fig. 5D) are not simply explained by the decrease of PSII/PSI ratio from the vegetative cells to the heterocysts, because Chl*a*: carotenoid number ratio of PSI (96:22 ≈ 4.36:1) is higher than that of and PSII (35:11 ≈ 3.18:1)

(Tables S3, S4). The observed low ratio (~0.35:1) is actually even lower than the lower limit (0.729:1 ≈ 3.18/4.36:1) given by a virtual conversion from 100% PSI in vegetative cells to 100% PSII in heterocysts, although these ratios are totally unrealistic for the two cell types (Table S8). It is thus likely that the ratio of carotenoids other than those bound in PSI or PSII have increased from vegetative cells to heterocysts of the subgroup B in the *Rivularia* filaments. Changes in carotenoid compositions of two heterocystous cyanobacteria (*Anabaena* sp. PCC7120 and *Calothrix* sp. 336/3) upon deprivation of exogenous combined nitrogen were reported [71]. Total β-carotene (including both trans and cis forms) was decreased from 37.6–42.5% to 27.4–31.5% while some of the other carotenoids (echinenone in both the species, zeaxanthin in only *Calothrix*) were increased. Although heterocysts and vegetative cells were not separately analyzed in the reference [71], these results may lead to the idea that the carotenoids not bound to PSI or PSII in the subgroup B of *Rivularia* heterocysts may be echinenone and/or zeaxanthin [72]. The frequency of the C=C stretching vibration (around 1520 cm^{-1}) of echinenone has been reported to be down shifted by about 5 cm^{-1} in comparison with β-carotene and zeaxanthin [73–75]. However, we did not detect clear change in the frequency between vegetative cells and heterocysts in both *A. variabilis* and *Rivularia* (Figs. 3, S2), suggesting that there is no strong localization of echinenone in the heterocysts. In spite of an elevated rate of respiration, thick cell wall and substantial decrease of PSII in the heterocysts, diffusion of O_2 through the terminal pore into the heterocysts and concomitant production of reactive oxygen species may be unavoidable [76]. The carotenoids in the *Rivularia* heterocyst other than those bound in PSI or small amount of PSII may be effective as a singlet oxygen quencher [77].

In view of the relatively high correlations between photoluminescence and carotenoid signals of the *Rivularia* heterocyst subgroups, the negligibly small correlation coefficient in the corresponding plot of *A. variabilis* heterocyst is remarkable (Fig. 5A, D). Some carotenoids not bound to PSI or small amount of PSII may accumulate in at least a portion of *A. variabilis* heterocysts (see also Section 3.5). It is also suggested that the ratio of total intracellular carotenoid to PSI in the heterocyst is more tightly regulated in *Rivularia* than in *A. variabilis*.

4.5. Implications for physiological status of vegetative cells in filamentous cyanobacteria

Some heterocystous cyanobacteria consist of vegetative cells with varied shapes and sizes, as in the case of *Rivularia* filaments (Fig. S1) [54,69,78]. In contrast, autofluorescence spectra as well as their sizes of vegetative cells of *Anabaena* and *Nostoc* are mostly very similar to each other [31,49,54,79]. For example, as far as we employed autofluorescence spectral microscopy and absorption spectral microscopy to analyze the individual vegetative cells near the heterocyst in *A. variabilis*, we were not able to detect convincing spectral differences between veg1 and veg2 (Table S6) [31,54]. On the other hand, some works reported at least transient appearance of abnormal vegetative cells [4,80]. Overall, our results and some previous studies indicate that transient and/or steady differences in the properties of thylakoid membranes between apparently similar vegetative cells are induced under some conditions.

All *A. variabilis* heterocysts we analyzed seemed to be already matured, because amounts of phycobilins in the heterocysts were on average only 6% of the average vegetative cell (Table 1, Fig. 5B, Table S2) [31]. PSI in some of the heterocysts may be decreased by aging of the heterocysts, because heterocyst is a terminally differentiated state (no possibility of division) and its lifetime is finite. The veg1 cell should be the candidate for the next terminal heterocyst cell, in which decrease of PSII-related photosynthetic pigments is expected if it is time for the terminal heterocyst to be replaced. Due possibly to the lack of synchronization in the culture and relatively long incubation time from the inoculation to the microscopic measurements (5–74 days for *A. variabilis*), we did not find correlation between the incubation time and the quantities of photosynthetic pigments in the heterocysts or veg1 cells (Fig. S6). More systematic tracking of the maturation or aging process of heterocysts is necessary to understand the physiological meaning of the special status of veg1 cell.

The mechanisms for the formation of the semiregularly spaced heterocyst positions among vegetative cells have been extensively studied [46,81]. Although many genes are involved in the differentiation process [82], the essential pattern formation and maintenance has been successfully reproduced by computer simulations considering several key genes and factors [83,84]. However, subtle differences between vegetative cells have not been paid much attention. The special status of the vegetative cells nearest to heterocysts (veg1) that we found (Table 1) may reflect a delicate balance among inhibitions of heterocyst differentiation in the vegetative cells, exchange of metabolites and signaling molecules between heterocysts and vegetative cells, aging of the heterocyst and cell division cycles in the vegetative cells [50,85].

5. Conclusions

The photoluminescence of Chl*a* (around 1017–1175 nm) in *A. variabilis* cells induced by the continuous wave laser at 976 nm seems to be fairly proportional to the concentration of Chl*a*. The photoluminescence spectrum was found to be almost common among the two cyanobacteria (*A. variabilis* and *Rivularia*), green alga and plant. Our analysis of the Raman bands of carotenoids, phycobilins and photoluminescence of Chl*a* supports the view that the phycobilisomes remain substantially in the *Rivularia* heterocysts, but only almost negligibly in *A. variabilis* heterocysts. At least two distinct physiological states of the terminal heterocyst in *Rivularia* filaments were distinguished by the correlations between the Raman bands of carotenoids and Chl*a*-associated photoluminescence, in which one state seems to be matured heterocyst and the other is relatively young heterocyst. The photoluminescence we observed by the continuous wave excitation at 976 nm is not something to be subtracted and neglected, but signals useful for analysis of chloroplasts and cyanobacteria on a single-cell basis. Some special roles of carotenoids other than those bound to PSI or small amount of PSII in both *A. variabilis* and *Rivularia* heterocysts are suggested through the photoluminescence/carotenoid correlations.

Transparency document

The Transparency document associated with this article can be found, in online version.

Acknowledgements

We thank Profs. Masahide Terazima (Kyoto Univ.), Haruo Inoue (Tokyo Metropolitan Univ.), Takashi Shiina (Kyoto Prefectural Univ.), Yoshifumi Kimura (Doshisha Univ.) and Hirozo Oh-Oka (Osaka Univ.) for valuable advice, Prof. Masanori Izumi (Tohoku Univ.) for providing *A. thaliana*. We also thank Dr. Shuho Nozue (King Abdullah Univ.) and Prof. Mitsunori Katayama (Nihon University) for their valuable contributions to our previous study that were highly relevant to this work.

Funding

This work was supported in part by the Japan Science and Technology Agency (the Precursory Research for Embryonic Science and Technology, “Chemical conversion of light energy”, to S.K.), MEXT-Supported Program for the Strategic Research Foundation at Private Universities (2015–2018, no. S1511025 partly to S.K.) and Molecular Science for Supra functional Systems (Area No.477, 19056012 to S.K.), JSPS KAKENHI (17H03968 partly to S.K. and 18K06153 partly to S.K.), the Murata Science Foundation (to S.K.), the Kyoto University Foundation (to S.K.) and Imaging Science Project of the Center for

Novel Science Initiatives (CNSI), National Institutes of Natural Sciences (NINS) (no. IS281001 to S.K.).

Appendix A. Supplementary data

Supplementary data to this article can be found online at https://doi.org/10.1016/j.bbabio.2018.11.012.

References

[1] B. Ke, Photosynthesis Photobiochemistry and Photobiophysics, Springer Science & Business Media, 2001.
[2] R.E. Blankenship, Molecular Mechanisms of Photosynthesis, John Wiley & Sons, 2014.
[3] K. Harter, A.J. Meixner, F. Schleifenbaum, Spectro-microscopy of living plant cells, Mol. Plant 5 (2012) 14–26.
[4] N. Ferimazova, K. Felcmanova, E. Setlikova, H. Kupper, I. Maldener, G. Hauska, B. Sediva, O. Prasil, Regulation of photosynthesis during heterocyst differentiation in *Anabaena* sp strain PCC 7120 investigated in vivo at single-cell level by chlorophyll fluorescence kinetic microscopy, Photosynth. Res. 116 (2013) 79–91.
[5] K. Omasa, A. Konishi, H. Tamura, F. Hosoi, 3D confocal laser scanning microscopy for the analysis of chlorophyll fluorescence parameters of chloroplasts in intact leaf tissues, Plant Cell Physiol. 50 (2009) 90–105.
[6] S. Kumazaki, M. Hasegawa, M. Ghoneim, Y. Shimizu, K. Okamoto, M. Nishiyama, H. Oh-Oka, M. Terazima, A line-scanning semi-confocal multi-photon fluorescence microscope with a simultaneous broadband spectral acquisition and its application to the study of the thylakoid membrane of a cyanobacterium *Anabaena* PCC7120, J. Microsc. (Oxford) 228 (2007) 240–254.
[7] Chlorophyll *a* Fluorescence: A Signature of Photosynthesis, Springer Netherlands, 2004.
[8] M.A. Amin, S. Nandi, P. Mondal, T. Mahata, S. Ghosh, K. Bhattacharyya, Physical chemistry in a single live cell: confocal microscopy, Phys. Chem. Chem. Phys. 19 (2017) 12620–12627.
[9] C.A. Bücherl, A. Bader, A.H. Westphal, S.P. Laptenok, J.W. Borst, FRET-FLIM applications in plant systems, Protoplasma 251 (2014) 383–394.
[10] S. Nozue, A. Mukuno, Y. Tsuda, T. Shiina, M. Terazima, S. Kumazaki, Characterization of thylakoid membrane in a heterocystous cyanobacterium and green alga with dual-detector fluorescence lifetime imaging microscopy with a systematic change of incident laser power, Biochim. Biophys. Acta, Bioenerg. 1857 (2016) 46–59.
[11] I. Iermak, J. Vink, A.N. Bader, E. Wientjes, H. van Amerongen, Visualizing heterogeneity of photosynthetic properties of plant leaves with two-photon fluorescence lifetime imaging microscopy, Biochim. Biophys. Acta, Bioenerg. 1857 (2016) 1473–1478.
[12] Govindjee, Chlorophyll *a* fluorescence: a bit of basics and history, in: C. Papageorgiou, Govindjee (Eds.), Chlorophyll *a* Fluorescence a Signature of Photosynthesis, Springer, Netherland, 2004, pp. 1–42.
[13] E. Kim, T.K. Ahn, S. Kumazaki, Changes in antenna sizes of photosystems during state transitions in granal and stroma-exposed thylakoid membrane of intact chloroplasts in *Arabidopsis* mesophyll protoplasts, Plant Cell Physiol. 56 (2015) 759–768.
[14] H.-O. Hamaguchi, Developments of Raman spectroscopy in the past 40 years: from a molecule to a living cell, Curr. Sci. 97 (2009) 186–191.
[15] H. Kandori, H. Sasabe, M. Mimuro, Direct determination of a lifetime of the S2 state of beta-carotene by femtosecond time-resolved fluorescence spectroscopy, J. Am. Chem. Soc. 116 (1994) 2671–2672.
[16] H. Hashimoto, K. Yanagi, M. Yoshizawa, D. Polli, G. Cerullo, G. Lanzani, S. De Silvestri, A.T. Gardiner, R.J. Cogdell, The very early events following photo-excitation of carotenoids, Arch. Biochem. Biophys. 430 (2004) 61–69.
[17] B. Robert, Resonance Raman studies in photosynthesis—chlorophyll and carotenoid molecules, Biophysical Techniques in Photosynthesis, Springer, 1996, pp. 161–176.
[18] W.F.J. Vermaas, J.A. Timlin, H.D.T. Jones, M.B. Sinclair, L.T. Nieman, S.W. Hamad, D.K. Melgaard, D.M. Haaland, In vivo hyperspectral confocal fluorescence imaging to determine pigment localization and distribution in cyanobacterial cells, Proc. Natl. Acad. Sci. U. S. A. 105 (2008) 4050–4055.
[19] M. Baranska, M. Roman, H. Schulz, R. Baranski, Recent advances in Raman analysis of plants: alkaloids, carotenoids, and polyacetylenes, Curr. Anal. Chem. 9 (2013) 108–127.
[20] X. Wei, D. Jie, J.J. Cuello, D.J. Johnson, Z. Qiu, Y. He, Microalgal detection by Raman microspectroscopy, TrAC Trends Anal. Chem. 53 (2014) 33–40.
[21] P. Vítek, C. Ascaso, O. Artieda, M.C. Casero, J. Wierzchos, Discovery of carotenoid red-shift in endolithic cyanobacteria from the Atacama Desert, Sci. Rep. 7 (2017) 11116.
[22] B. DemmigAdams, A.M. Gilmore, W.W. Adams, Carotenoids 3. In vivo functions of carotenoids in higher plants, FASEB J. 10 (1996) 403–412.
[23] C.I. Cazzonelli, Carotenoids in nature: insights from plants and beyond, Funct. Plant Biol. 38 (2011) 833–847.
[24] A.V. Ruban, Nonphotochemical chlorophyll fluorescence quenching: mechanism and effectiveness in protecting plants from photodamage, Plant Physiol. 170 (2016) 1903–1916.
[25] S.-G. Kong, M. Wada, Recent advances in understanding the molecular mechanism of chloroplast photorelocation movement, Biochim. Biophys. Acta, Bioenerg. 1837 (2014) 522–530.
[26] Y. Huang, C. Beal, W. Cai, R. Ruoff, E. Terentjev, Micro-Raman spectroscopy of algae: composition analysis and fluorescence background behavior, Biotechnol. Bioeng. 105 (2010) 889–898.
[27] B. Gobets, R. van Grondelle, Energy transfer and trapping in photosystem I, BBA-Bioenergetics 1507 (2001) 80–99.
[28] A. Thapper, F. Mamedov, F. Mokvist, L. Hammarstrom, S. Styring, Defining the far-red limit of photosystem II in spinach, Plant Cell 21 (2009) 2391–2401.
[29] M. Hasegawa, T. Shiina, M. Terazima, S. Kumazaki, Selective excitation of photosystems in chloroplasts inside plant leaves observed by near-infrared laser-based fluorescence spectral microscopy, Plant Cell Physiol. 51 (2010) 225–238.
[30] M. Hasegawa, T. Yoshida, M. Yabuta, M. Terazima, S. Kumazaki, Anti-stokes fluorescence spectra of chloroplasts in *Parachlorella kessleri* and maize at room temperature as characterized by near-infrared continuous-wave laser fluorescence microscopy and absorption microscopy, J. Phys. Chem. B 115 (2011) 4184–4194.
[31] S. Kumazaki, M. Akari, M. Hasegawa, Transformation of thylakoid membranes during differentiation from vegetative cell into heterocyst visualized by microscopic spectral imaging, Plant Physiol. 161 (2013) 1321–1333.
[32] F. Mokvist, F. Mamedov, S. Styring, Defining the far-red limit of photosystem I the primary charge separation is functional to 840 nm, J. Biol. Chem. 289 (2014) 24630–24639.
[33] M. Ando, M. Sugiura, H. Hayashi, H.-o. Hamaguchi, 1064 nm deep near-infrared (NIR) excited Raman microspectroscopy for studying photolabile organisms, Appl. Spectrosc. 65 (2011) 488–492.
[34] H. Wu, J.V. Volponi, A.E. Oliver, A.N. Parikh, B.A. Simmons, S. Singh, In vivo lipidomics using single-cell Raman spectroscopy, Proc. Natl. Acad. Sci. U. S. A. 108 (2011) 3809–3814.
[35] B. Schrader, H. Klump, K. Schenzel, H. Schulz, Non-destructive NIR FT Raman analysis of plants, J. Mol. Struct. 509 (1999) 201–212.
[36] H.G. Edwards, E.M. Newton, D.L. Dickensheets, D.D. Wynn-Williams, Raman spectroscopic detection of biomolecular markers from Antarctic materials: evaluation for putative Martian habitats, Spectrochim. Acta A Mol. Biomol. Spectrosc. 59 (2003) 2277–2290.
[37] R. Baranski, M. Baranska, H. Schulz, Changes in carotenoid content and distribution in living plant tissue can be observed and mapped in situ using NIR-FT-Raman spectroscopy, Planta 222 (2005) 448–457.
[38] D.M. Gates, H.J. Keegan, J.C. Schleter, V.R. Weidner, Spectral properties of plants, Appl. Opt. 4 (1965) 11–20.
[39] R. Loudon, The Quantum Theory of Light, Oxford University Press, 2000.
[40] S. York, InGaAs SWIR cameras open new opportunities, Photonics Spectra, 48 2014, pp. 55–58.
[41] K.F. Palmer, D. Williams, Optical properties of water in the near infrared*, J. Opt. Soc. Am. 64 (1974) 1107–1110.
[42] Z. Pilát, J. Ježek, M. Šerý, M. Trtílek, L. Nedbal, P. Zemánek, Optical trapping of microalgae at 735–1064 nm: photodamage assessment, J. Photochem. Photobiol. B Biol. 121 (2013) 27–31.
[43] Y. Kamei, M. Suzuki, K. Watanabe, K. Fujimori, T. Kawasaki, T. Deguchi, Y. Yoneda, T. Todo, S. Takagi, T. Funatsu, Infrared laser–mediated gene induction in targeted single cells in vivo, Nat. Methods 6 (2009) 79.
[44] R. Haselkorn, Heterocysts, Annu. Rev. Plant Physiol. Plant Mol. Biol. 29 (1978) 319–344.
[45] C. Wolk, A. Ernst, J. Elhai, Heterocyst metabolism and development, in: B. D (Ed.), The Molecular Biology of Cyanobacteria, Kluwer Academic Publisher, Netherland, 1994, pp. 769–823.
[46] A. Herrero, J. Stavans, E. Flores, The multicellular nature of filamentous heterocyst-forming cyanobacteria, FEMS Microbiol. Rev. 40 (2016) 831–854.
[47] A. Magnuson, T. Cardona, Thylakoid membrane function in heterocysts, Biochim. Biophys. Acta, Bioenerg. 1857 (2016) 309–319.
[48] L. Ying, X. Huang, B. Huang, J. Xie, J. Zhao, X.S. Zhao, Fluorescence emission and absorption spectra of single *Anabaena* sp. strain PCC7120 cells, Photochem. Photobiol. 76 (2002) 310–313.
[49] K. Sugiura, S. Itoh, Single-cell confocal spectrometry of a filamentous cyanobacterium *Nostoc* at room and cryogenic temperature. Diversity and differentiation of pigment systems in 311 cells, Plant Cell Physiol. 53 (2012) 1492–1506.
[50] M. Toyoshima, N.V. Sasaki, M. Fujiwara, S. Ehira, M. Ohmori, N. Sato, Early candidacy for differentiation into heterocysts in the filamentous cyanobacterium *Anabaena* sp. PCC 7120, Arch. Microbiol. 192 (2010) 23–31.
[51] S. Ke, R. Haselkorn, Fluorescence spectroscopy study of heterocyst differentiation in *Anabaena* PCC 7120 filaments, Microbiology 159 (2013) 253–258.
[52] J. Ishihara, M. Tachikawa, A. Mochizuki, Y. Sako, H. Iwasaki, S. Morita, Raman imaging of the diverse states of the filamentous cyanobacteria, Nano-Bio Sensing, Imaging and Spectroscopy, International Society for Optics and Photonics, 2013(pp. 88790V-88790V-88794).
[53] A. Dementjev, J. Kostkeviciene, Applying the method of coherent anti-stokes Raman microscopy for imaging of carotenoids in microalgae and cyanobacteria, J. Raman Spectrosc. 44 (2013) 973–979.
[54] S. Nozue, M. Katayama, M. Terazima, S. Kumazaki, Comparative study of thylakoid membranes in terminal heterocysts and vegetative cells from two cyanobacteria, Rivularia M-261 and *Anabaena variabilis*, by fluorescence and absorption spectral microscopy, Biochim. Biophys. Acta, Bioenerg. 1858 (2017) 742–749.
[55] R.Y. Stanier, R. Kunisawa, M. Mandel, G. Cohenbaz, Purification and properties of unicellular blue-green algae (order Chroococcales), Bacteriol. Rev. 35 (1971) 171.
[56] J.C. Meeks, J. Elhai, Regulation of cellular differentiation in filamentous cyanobacteria in free-living and plant-associated symbiotic growth states, Microbiol. Mol. Biol. Rev. 66 (2002) 94–121.
[57] S.F. Parker, S.M. Tavender, N.M. Dixon, H. Herman, K.P.J. Williams, W.F. Maddams, Raman spectrum of beta-carotene using laser lines from green

(514.5 nm) to near-infrared (1064 nm): implications for the characterization of conjugated polyenes, Appl. Spectrosc. 53 (1999) 86–91.
[58] C. Kneip, A. Parbel, H. Foerstendorf, H. Scheer, F. Siebert, P. Hildebrandt, Fourier transform near-infrared resonance Raman spectroscopic study of the α-subunit of phycoerythrocyanin and phycocyanin from the cyanobacterium *Mastigocladus laminosus*, J. Raman Spectrosc. 29 (1998) 939–944.
[59] H. Sato, K. Okada, K. Uehara, Y. Ozaki, Near-infrared Fourier-transform Raman study of chlorophyll *a* in solutions, Photochem. Photobiol. 61 (1995) 175–182.
[60] W.A. Sidler, Phycobilisome and phycobiliprotein structures, The Molecular Biology of Cyanobacteria, Springer, 1994, pp. 139–216.
[61] M. Watanabe, D.A. Semchonok, M.T. Webber-Birungi, S. Ehira, K. Kondo, R. Narikawa, M. Ohmori, E.J. Boekema, M. Ikeuchi, Attachment of phycobilisomes in an antenna–photosystem I supercomplex of cyanobacteria, Proc. Natl. Acad. Sci. 111 (2014) 2512–2517.
[62] M. Donahue, H. Huang, C. Brouillette, W. Smith, S. Farquharson, Detecting explosives by portable Raman analyzers: a comparison of 785-, 976-, 1064-, and 1550-nm (retina-safe) laser excitation, Spectroscopy (2011), http://www.spectroscopyonline.com/detecting-explosives-portable-raman-analyzers-comparison-785-976-1064-and-1550-nm-retina-safe-laser?id=&pageID=1&sk=&date=.
[63] D.A. Hartzler, D.M. Niedzwiedzki, D.A. Bryant, R.E. Blankenship, Y. Pushkar, S. Sayikhin, Triplet excited state energies and phosphorescence spectra of (bacterio) chlorophylls, J. Phys. Chem. B 118 (2014) 7221–7232.
[64] G.C. Righini, M. Ferrari, Photoluminescence of rare-earth-doped glasses, Riv. Nuovo Cimento 28 (2005) 1–53.
[65] M. Howard-Azzeh, L. Shamseer, H.E. Schellhorn, R.S. Gupta, Phylogenetic analysis and molecular signatures defining a monophyletic clade of heterocystous cyanobacteria and identifying its closest relatives, Photosynth. Res. 122 (2014) 171–185.
[66] A. Krasnovsky, Y.V. Kovalev, Spectral and kinetic parameters of phosphorescence of triplet chlorophyll a in the photosynthetic apparatus of plants, Biochem. Mosc. 79 (2014) 349–361.
[67] A. Telfer, Singlet oxygen production by PSII under light stress: mechanism, detection and the protective role of beta-carotene, Plant Cell Physiol. 55 (2014) 1216–1223.
[68] C. Triantaphylidès, M. Havaux, Singlet oxygen in plants: production, detoxification and signaling, Trends Plant Sci. 14 (2009) 219–228.
[69] B.A. Whitton, P. Mateo, Rivulariaceae, in: B.A. Whitton (Ed.), Ecology of Cyanobacteria II: Their Diversity in Space and Time, Springer Science + Business Media, 2012.
[70] D.G. Adams, P.S. Duggan, Heterocyst and akinete differentiation in cyanobacteria, New Phytol. 144 (1999) 3–33.
[71] S. Kosourov, G. Murukesan, J. Jokela, Y. Allahverdiyeva, Carotenoid biosynthesis in *Calothrix* sp. 336/3: composition of carotenoids on full medium, during diazotrophic growth and after long-term H2 photoproduction, Plant Cell Physiol. 57 (2016) 2269–2282.
[72] P. Fromme, P. Jordan, N. Krauß, Structure of photosystem I, Biochim. Biophys. Acta, Bioenerg. 1507 (2001) 5–31.
[73] E. Kish, M.M.M. Pinto, D. Kirilovsky, R. Spezia, B. Robert, Echinenone vibrational properties: from solvents to the orange carotenoid protein, Biochim. Biophys. Acta, Bioenerg. 1847 (2015) 1044–1054.
[74] L.F. Maia, R.F. Fernandes, G. Lobo-Hajdu, L.F. de Oliveira, Conjugated polyenes as chemical probes of life signature: use of Raman spectroscopy to differentiate polyenic pigments, Phil. Trans. R. Soc. A 372 (2014) 20140200.
[75] J. Jehlička, H.G. Edwards, K. Osterrothová, J. Novotná, L. Nedbalová, J. Kopecký, I. Němec, A. Oren, Potential and limits of Raman spectroscopy for carotenoid detection in microorganisms: implications for astrobiology, Phil. Trans. R. Soc. A 372 (2014) 20140199.
[76] A.E. Walsby, Cyanobacterial heterocysts: terminal pores proposed as sites of gas exchange, Trends Microbiol. 15 (2007) 340–349.
[77] R. Edge, D. McGarvey, T. Truscott, The carotenoids as anti-oxidants—a review, J. Photochem. Photobiol. B Biol. 41 (1997) 189–200.
[78] Á.M. Plominsky, J. Larsson, B. Bergman, N. Delherbe, I. Osses, M. Vásquez, Dinitrogen fixation is restricted to the terminal heterocysts in the invasive cyanobacterium *Cylindrospermopsis raciborskii* CS-505, PLoS One 8 (2013) e51682.
[79] S. Ke, V. Bindokas, R. Haselkorn, *Anabaena* cell ageing monitored with confocal fluorescence spectroscopy, Microbiology 161 (2015) 84–88.
[80] T. Cardona, N. Battchikova, Å. Agervald, P. Zhang, E. Nagel, E.-M. Aro, S. Styring, P. Lindblad, A. Magnuson, Isolation and characterization of thylakoid membranes from the filamentous cyanobacterium *Nostoc punctiforme*, Physiol. Plant. 131 (2007) 622–634.
[81] L. Corrales-Guerrero, V. Mariscal, D.J. Nurnberg, J. Elhai, C.W. Mullineaux, E. Flores, A. Herrero, Subcellular localization and clues for the function of the HetN factor influencing heterocyst distribution in *Anabaena* sp strain PCC 7120, J. Bacteriol. 196 (2014) 3452–3460.
[82] S. Ehira, Transcriptional regulation of heterocyst differentiation in *Anabaena* sp. strain PCC 7120, Russ. J. Plant Physiol. 60 (2013).
[83] A. Torres-Sánchez, J. Gómez-Gardeñes, F. Falo, An integrative approach for modeling and simulation of heterocyst pattern formation in cyanobacteria filaments, PLoS Comput. Biol. 11 (2015) e1004129.
[84] J. Muñoz-García, S. Ares, Formation and maintenance of nitrogen-fixing cell patterns in filamentous cyanobacteria, Proc. Natl. Acad. Sci. 113 (2016) 6218–6223.
[85] C.W. Mullineaux, V. Mariscal, A. Nenninger, H. Khanum, A. Herrero, E. Flores, D.G. Adams, Mechanism of intercellular molecular exchange in heterocyst-forming cyanobacteria, EMBO J. 27 (2008) 1299–1308.